

Pump-probe optical spectroscopy of hexagonal YMnO₃ over wide time and energy rangesTakuro Katsufuji^{1,2}, Taishi Yoshida,¹ Kaoru Akimoto,¹ So Okubo,¹ and Takuo Saiki¹¹*Department of Physics, Waseda University, Tokyo 169-8555, Japan*²*Kagami Memorial Research Institute for Materials Science and Technology, Waseda University, Tokyo 169-0051, Japan*

(Received 13 April 2023; revised 21 June 2023; accepted 11 September 2023; published 21 September 2023)

To study the photoinduced processes in strongly correlated electron systems occurring coherently on various time scales, we conducted the pump-probe optical spectroscopy of hexagonal YMnO₃ with ranges of delay time between 0.1 and 5000 ps and the energy of light between 1 and 3 eV. We found that the photoinduced changes in reflectivity were dominated by the intra-atomic excitation of a *d* electron in Mn, by the relaxation of energy from electronic excitations to phonon excitations, by the propagation of a strain wave, and by thermal conduction inside a sample, which occur successively with time. We also found that the sound velocity and thermal conductivity of the sample including their anisotropy can be obtained by this technique.

DOI: [10.1103/PhysRevB.108.125131](https://doi.org/10.1103/PhysRevB.108.125131)**I. INTRODUCTION**

Time-resolved spectroscopy is a powerful experimental technique for studying both the equilibrium and nonequilibrium states of matter. One of the experimental techniques of time-resolved spectroscopy is pump-probe optical measurement [1–8], where the first laser pulse excites the electron in a sample and the second laser pulse with a time delay measures the optical properties of the sample. This technique has been applied to various types of material, including transition metal compounds as strongly correlated electron systems. For such strongly correlated electron systems, the most prominent phenomena observed by this technique are photoinduced phase transitions; the first pulse applied to the sample induces a phase transition in the sample, which can be detected by the second pulse. Various types of phase transition, for example, the Mott transition [1,2,4,6], charge ordering [3,5], and orbital ordering [7], have been induced or melted by the application of laser pulses.

In pump-probe measurements, different phenomena occur on different time scales. For example, (1) the excitation of electrons by a pump pulse induces the reconstruction of electronic states in less than 10^{-12} s (corresponding to several meV in energy), which is governed by the electron bandwidth. Subsequently, (2) the excited electrons are relaxed and the energy is transferred to the phonon excitations, resulting in the increase in the temperature of the lattice within several 10^{-12} s, which is dominated by the frequency of phonons. If a photoinduced phase transition occurs at this stage, it is accompanied by a strain in the lattice, which propagates through the velocity of sound waves. Even in the absence of photoinduced phase transitions, the expansion of the lattice caused by the increase in the temperature of the lattice generates a strain wave propagating through the sound velocity. Therefore, (3) the propagation of such a strain wave results in the time-dependent interference of the light reflected at the sample surface and the wave front of the strain wave [9–11]. On the basis of the wavelength of the light (typically $\sim 5 \times 10^{-7}$ m) and sound velocity (typically $\sim 5 \times 10^3$ m/s), the oscillation of

reflectivity with a period of typically several 10^{-11} s appears. Finally, (4) the temperature of the lattice decreases because of thermal conduction in the sample. A typical time scale of this process is given by the diffusion length of heat becoming comparable to the penetration depth of the pump pulse and, since the typical thermal diffusivity of, for example, oxides is $\sim 10^{-6}$ m²/s and the penetration depth of light is typically $\sim 10^{-7}$ m, a change in reflectivity over a time scale of 10^{-8} s can appear [12–16].

Note that each of processes (1)–(4) above has its own anisotropy with respect to not only the polarization direction of light but also the direction of the sample surface on which a pump pulse is applied. Recently, it has been found that a photoinduced phase transition in Ti₃O₅ is contingent on the relationship between the direction of the *c* axis, which exhibits a large change with a phase transition and the direction of the sample surface on which a pump pulse is applied [8]. This relationship is dominated by the strain of the crystal and is thus related to process (3), but a similar anisotropy with respect to the sample surface is expected for process (4) because of the anisotropy of the thermal conductivity of the sample.

It should also be pointed out that each process with its own time scale has been studied in specific materials thus far, but the study of the processes on various time scales in a single material has been limited. In this paper, we conducted multi-time-scale (from $t = 1 \times 10^{-13}$ to 5×10^{-9} s) and wide-energy-range (from $\hbar\omega = 1$ to 3 eV) time-resolved optical spectroscopy on two different surfaces of a sample to study all the processes from (1) to (4) including their anisotropy on the same material.

The compound studied here is hexagonal YMnO₃, one of a series of hexagonal RMnO₃ (*R*: rare earth) known to exhibit both ferroelectric and magnetic ordering [17–19]. This series of compound is characterized by a quasitriangular lattice of Mn³⁺ ions ($3d^4$) surrounded by three in-plane oxygen ions and two apical oxygen ions. The $3d$ orbitals of Mn are thus split into the doubly degenerate *yz* and *zx* states, the

doubly degenerate xy and $x^2 - y^2$ states, and the nondegenerate $3z^2 - r^2$ state, in order of increasing energy [17,20]. There is a sharp peak at ~ 1.6 eV in the optical conductivity spectrum [20] and it corresponds to the intra-atomic excitations of a d electron from the $xy/x^2 - y^2$ states to the $3z^2 - r^2$ state. This peak has been the main focus of studies on this material by pump-probe spectroscopy [21–28], although there has been a lack of extensive analysis of these spectra over a wide range of $\hbar\omega$. Furthermore, processes (3) and (4) in YMnO_3 have barely been studied, although the sound velocity [29] and thermal conductivity [30] including their anisotropy have been measured in YMnO_3 by conventional techniques. It would be valuable to compare the values obtained by the spectroscopic technique with those obtained by conventional techniques.

II. EXPERIMENT

A single crystal of YMnO_3 was grown by the floating-zone technique [18]. The crystal orientation was determined using the Laue method and the crystal was cut and polished along both the ac and ab planes with alumina powder. Pump-probe optical spectroscopy was performed using a Ti:sapphire regenerative amplified laser (with a pulse width of 130 fs, a repetition rate of 1 kHz, and a wavelength of 795 nm). A pump pulse with power density of typically 6 mJ/cm^2 was applied to the crystal and a probe pulse, whose frequency was broadened between $\hbar\omega = 1$ and 3 eV by focusing the laser pulse into the circulating water within the optical cell, was focused onto the sample surface. The reflected light was monochromated using a monochromator and detected using a Si photodiode. The time delay between the pump and probe pulses was controlled by varying the difference in optical path length using an optical stage and measurements were conducted with a time delay from 0.1 ps to 5 ns (equivalent to $\sim 1.5 \text{ m}$ in length). Care was taken to ensure that the intensity profile of the laser spot on the sample surface does not change when the stage was moved by such a long distance. The typical time resolution dominated by the width of the probe pulse was 0.3 ps in the present measurements. The polarization of both the pump and probe pulses was set along the a axis owing to the fact that the optical conductivity spectrum of this compound along the ab plane exhibits a sharp peak at ~ 1.6 eV, whereas the spectrum along the c axis is structureless below 3 eV. All the pump-probe measurements have been carried out at room temperature.

III. RESULTS

First, as an example of the results obtained over the entire time range of the present experiment, the photoinduced $\Delta R/R$ of YMnO_3 at $\hbar\omega = 1.4$ eV of the probe pulse as a function of the delay time t from 0.1 to 5000 ps on a log scale is shown in Fig. 1. The ranges indicated by numbers (1)–(4) approximately correspond to processes (1)–(4) in the Introduction, as described below.

Figures 2(a) and 2(b) show the photoinduced changes in the reflectivity spectra $\Delta R/R$ for YMnO_3 on the ac and ab planes at various values of delay time t . As can be seen, sharp structures exist between 1 and 2 eV in the photoinduced $\Delta R/R$ spectrum. Note that the $\Delta R/R$ spectrum at $t = 0.3$ ps is different from the spectra at $t \geq 1$ ps.

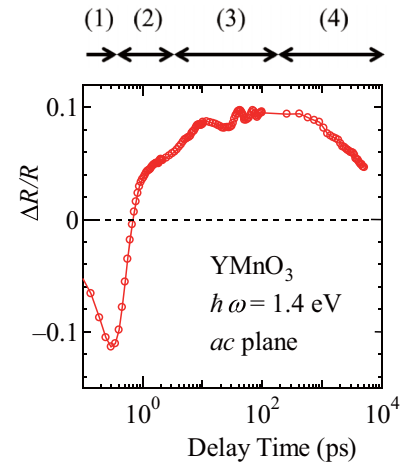


FIG. 1. Photoinduced change in the reflectivity $\Delta R/R$ at $\hbar\omega = 1.4$ eV of the probe pulse on the ac plane as a function of the delay time t on a log scale.

Figures 3(a) and 3(b) show the t dependence of the photoinduced $\Delta R/R$ at various $\hbar\omega$ values of the probe pulse up to 10 ps on the ac and ab planes. $\Delta R/R$ at $t > 10$ ps will be discussed later. At several $\hbar\omega$ values, $\Delta R/R$ markedly changes from negative to positive (at $\hbar\omega = 1.4$ eV, for example) or from positive to negative (at $\hbar\omega = 1.8$ eV, for example) within 2 ps. These results are consistent with the $\Delta R/R$ spectra at various t values shown in Fig. 2. Note that, although some of these results have already been reported in previous papers on hexagonal RMnO_3 [21–28], the photoinduced $\Delta R/R$ spectra over a wide $\hbar\omega$ range (1–3 eV) at various t values (0.1–5000 ps) have not been measured thus far.

The photoinduced $\Delta R/R$ spectra at $t \leq 10$ ps measured on the ac plane and those on the ab plane shown in Fig. 2, as well as the t dependence of the photoinduced $\Delta R/R$ up to 10 ps measured on the ac plane and that on the ab plane in Fig. 3, are similar, except for a small difference caused by a different behavior of a strain wave, as discussed later, and by experimental error. Thus we discuss the spectra on the ab plane below. To understand the photoinduced $\Delta R/R$ spectra at various t values, we analyzed the data as follows. First, we measured the reflectivity spectrum of YMnO_3 with the polarization direction along the ab plane [Fig. 4(a)] and

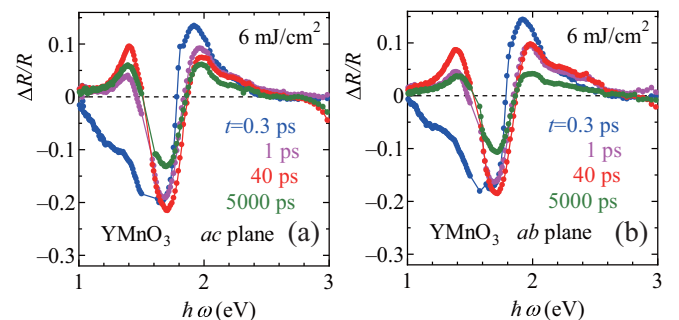


FIG. 2. Photoinduced changes in the reflectivity spectra $\Delta R/R$ at various values of delay time t on the (a) ac and (b) ab planes for YMnO_3 .

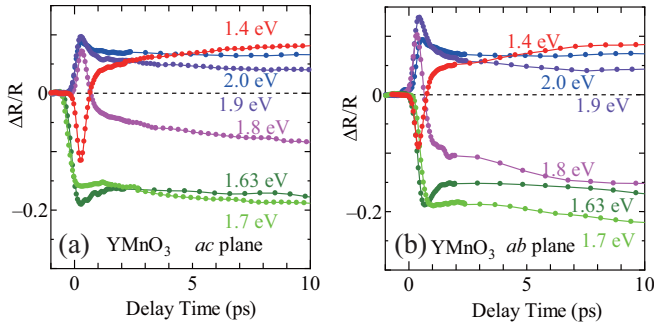


FIG. 3. Photoinduced change in the reflectivity $\Delta R/R$ as a function of the delay time t at various values of $\hbar\omega$ of the probe pulse on the (a) ac and (b) ab planes.

obtained the optical conductivity spectrum by the Kramers-Kronig transformation of the reflectivity spectrum [Fig. 4(b)]. Next, we fit the optical conductivity spectrum using Lorentz functions:

$$\epsilon(\omega) = \epsilon_{\infty} + \sum_{i=1} \frac{S_i \omega_i^2}{\omega_i^2 - \omega^2 - i\omega\gamma_i}, \quad (1)$$

$$\sigma(\omega) = \text{Im}\{\omega\epsilon(\omega)\}. \quad (2)$$

As shown in Fig. 4(b), the optical conductivity spectrum of YMnO_3 along the ab plane between 0 and 3 eV can be fitted using two Lorentz functions, one corresponding to a sharp peak at 1.6 eV and the other corresponding to a broad peak at ~ 5 eV. Finally, the parameters of the two Lorentz functions were shifted so that the change in reflectivity calculated using

$$R(\omega) = \left| \frac{\sqrt{\epsilon(\omega)} - 1}{\sqrt{\epsilon(\omega)} + 1} \right|^2 \quad (3)$$

reproduces the experimentally obtained photoinduced $\Delta R/R$ spectra.

Figures 5(a)–5(c) show the thus-obtained $\Delta R/R$ spectra as solid lines. Furthermore, the optical conductivity spectra obtained by the fitting are shown in Fig. 5(d). As can be seen, the height of the peak centered at 1.6 eV in the optical conductivity spectra decreases and the width increases for the spectrum at $t = 0.3$ ps compared with that before the application of the pump pulse (< 0 ps). On the other hand,

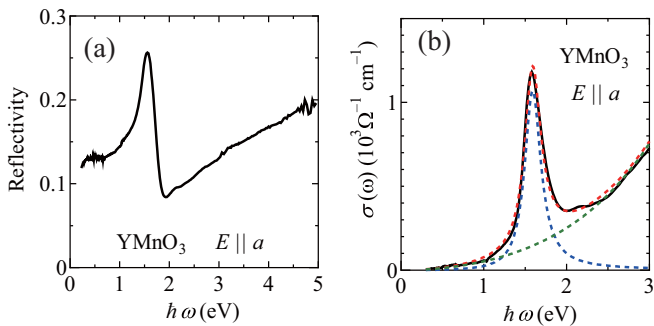


FIG. 4. (a) Reflectivity spectrum with $E \parallel a$ for YMnO_3 . (b) Optical conductivity spectrum obtained by the Kramers-Kronig transformation of the reflectivity spectrum. Dashed lines are the results of the fitting using two Lorentz functions.

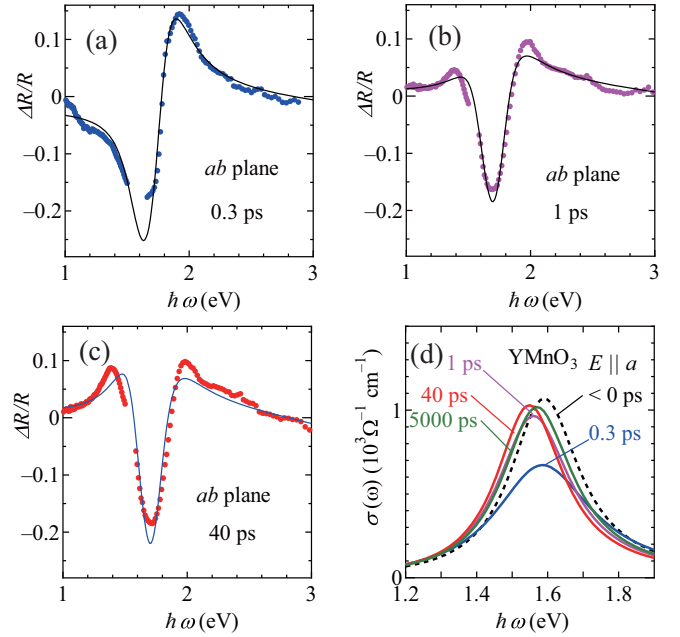


FIG. 5. (a)–(c) Fitting of the photoinduced changes in the reflectivity spectra $\Delta R/R$ at (a) 0.3, (b) 1, and (c) 40 ps. The solid circles are the experimental results and the solid lines are the results of the fitting. (d) Change in Lorentz function for the intra-atomic excitation of the d electron obtained by the fitting at each t .

the height and width become comparable to those at < 0 ps but the peak frequency shifts to lower values for the spectra at $t \geq 1$ ps. The changes in parameters for the peak at 1.6 eV obtained by the fitting are plotted as a function of t in Fig. 6. As can be seen, the width γ_1 , which is ~ 0.24 eV before the application of a pump pulse, increases by 0.1 eV immediately

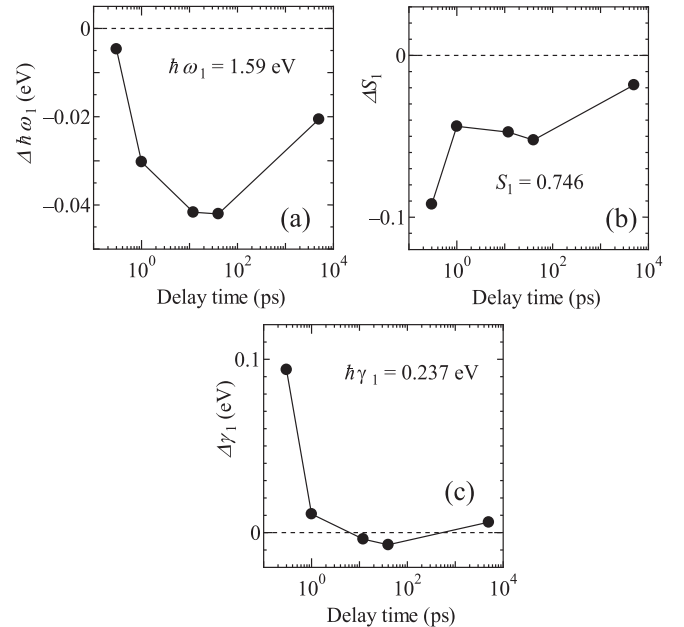


FIG. 6. Changes in the parameters of the Lorentz function, (a) the peak position $\hbar\omega_1$, (b) the spectral weight of the peak S_1 , and (c) the width of the peak γ_1 as functions of the delay time t .

after the application of a pump pulse. However, this increase in γ_1 almost disappears within 1 ps; alternatively, the peak frequency $\hbar\omega_1$ shifts to smaller values by ~ 0.03 eV at $t = 1$ ps and further shifts (by ~ 0.04 eV in total) at $t = 10$ ps.

The broadening of the peak at 1.6 eV occurs in less than 0.3 ps but disappears at 1 ps, indicating that it is dominated solely by the electronic process. As discussed in the Introduction, this peak corresponds to the excitation of Mn 3*d* electrons from the $xy/x^2 - y^2$ states to the $3z^2 - r^2$ state and the broadening of the peak for such excitation may be caused by the coupling of the peak with other electronic excitations. As seen in Fig. 4(b), in addition to the sharp peak at 1.6 eV, there is a broad background starting from $\hbar\omega \sim 1$ eV to higher $\hbar\omega$ values, which is due to the so-called charge-transfer excitation from the oxygen 2*p* states to the Mn 3*d* states. It is likely that this excitation is coupled with the local excitation of the *d* electrons in the Mn ions. If we excite electrons from the $xy/x^2 - y^2$ states to the $3z^2 - r^2$ state using the pump pulse, the population of electrons in the *d* orbitals of the Mn ions changes, which causes the redistribution of electrons through coupling with the charge-transfer excitation including the oxygen 2*p* states. We speculate that such redistribution of electrons is the origin of the broadening of the 1.6 eV peak at $t = 0.3$ ps as shown in Fig. 6(c). On the other hand, the peak at 1.6 eV in the optical conductivity spectrum of RMnO₃ is known to shift to higher frequencies with decreasing *T* [20]. This indicates that the shift of the peak at 1.6 eV to lower frequencies at $t > 1$ ps after the application of a pump pulse shown in Fig. 6(a) is caused by the increase in lattice temperature. Note that the amount of shift of the peak is suppressed from 40 to 5000 ps, as shown in Fig. 6(a), resulting in the decrease in the absolute value of $\Delta R/R$ with increasing *t* as shown in Fig. 2, which is due to the thermal conduction inside the sample, as discussed later.

As already discussed, the difference between $\Delta R/R$ with $E_{\text{pump}} \parallel a$ and $E_{\text{probe}} \parallel a$ (where E_{pump} and E_{probe} correspond to the polarization directions of the pump and probe pulses, respectively) on the *ac* plane and that on the *ab* plane is barely observed for $t < 10$ ps. Note that the two measurements on different planes of the crystal have to be conducted in different configurations; thus it is difficult to precisely reproduce the optical path, causing a large error, thereby preventing the detection of the anisotropy in these measurements. In this respect, we also investigated another anisotropy in the direction of the polarization for the pump and probe pulses, namely, the difference between $\Delta R/R$ with $E_{\text{pump}} \parallel a$ and $E_{\text{probe}} \parallel a$ and that with $E_{\text{pump}} \parallel a$ and $E_{\text{probe}} \parallel b$, where *b* corresponds to the direction perpendicular to both *c* and *a*, on the *ab* plane. In this case, the measurements can be conducted without changing the optical path but by simply rotating the polarization direction; thus it is possible to compare the anisotropy more precisely than in the case where the configurations of the crystal have to be changed. Figures 7(a)–7(c) show the photoinduced $\Delta R/R$ with $E_{\text{pump}} \parallel a$ and $E_{\text{probe}} \parallel a$ and that with $E_{\text{pump}} \parallel a$ and $E_{\text{probe}} \parallel b$, together with the difference between the two at $\hbar\omega_{\text{probe}} = 1.4, 1.63,$ and 2.0 eV. As can be seen, however, no sign of anisotropy is observed even in these measurements. This means that even if anisotropy occurs immediately after the application of a pump pulse owing to its polarization direction, such anisotropy is suppressed in

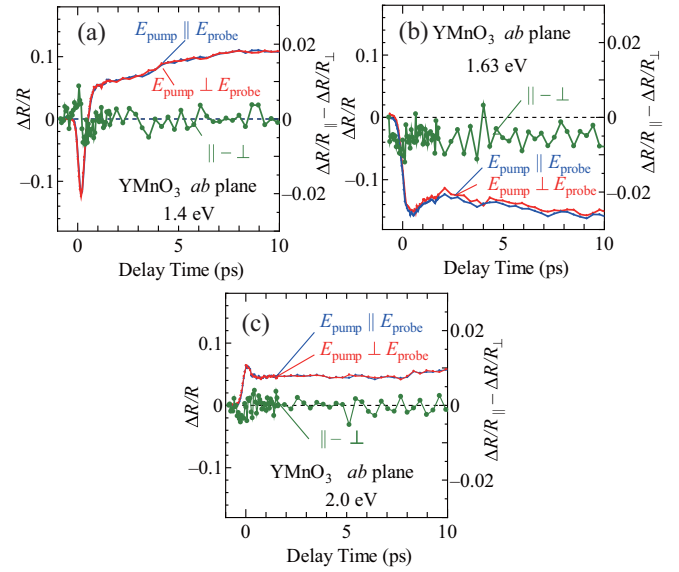


FIG. 7. Photoinduced change in the reflectivity $\Delta R/R$ as a function of the delay time t with $E_{\text{pump}} \parallel a$, $E_{\text{probe}} \parallel a$ (blue) and with $E_{\text{pump}} \parallel a$, $E_{\text{probe}} \parallel b$ (red) on the left axis and the difference between the two (green) on the right axis when $\hbar\omega$ of the probe pulse is (a) 1.4, (b) 1.63, and (c) 2.0 eV.

less than 1 ps due to the coupling of the intra-atomic excitation of the *d* electron with the charge-transfer excitation.

Next, let us discuss $\Delta R/R$ up to several tens of picoseconds. A typical time dependence of $\Delta R/R$ in this time range, including its anisotropy between that measured on the *ac* plane and that on the *ab* plane, is shown in Fig. 8(a). As can be seen, the oscillation of $\Delta R/R$ with t is clearly observed and the oscillation period is longer on the *ab* plane. This type of oscillation in the photoinduced $\Delta R/R$ has been often observed and assigned to the strain wave [9–11]. This means that, with the application of a pump pulse to the sample surface, the temperature of the lattice suddenly increases, resulting in the expansion of the crystal only over the penetration depth of the pump pulse. Subsequently, the increased volume of the crystal propagates perpendicular to the sample surface with the sound velocity of the crystal in a longitudinal mode. Because of the interference between the reflected light of the probe pulse at the sample surface and that reflected at the wave front of the strain wave, which propagates with time through the sound velocity, the oscillation of $\Delta R/R$ with time appears. In this model, the period of the oscillation T is given by

$$T = \frac{2n\lambda}{v}, \quad (4)$$

where n is the refractive index of the material at $\hbar\omega_{\text{probe}}$, λ is the wavelength of the probe pulse in vacuum ($= 2\pi c/\omega_{\text{probe}}$, where c is the light speed), and v is the sound velocity perpendicular to the sample surface. Although n depends on the direction of the polarization of the probe pulse, since it is along the *a* axis both on the *ac* and *ab* planes in this experiment, the difference between v along the *a* axis (corresponding to the result on the *ac* plane) and that along the *c* axis (corresponding to the result on the *ab* plane) is the origin of

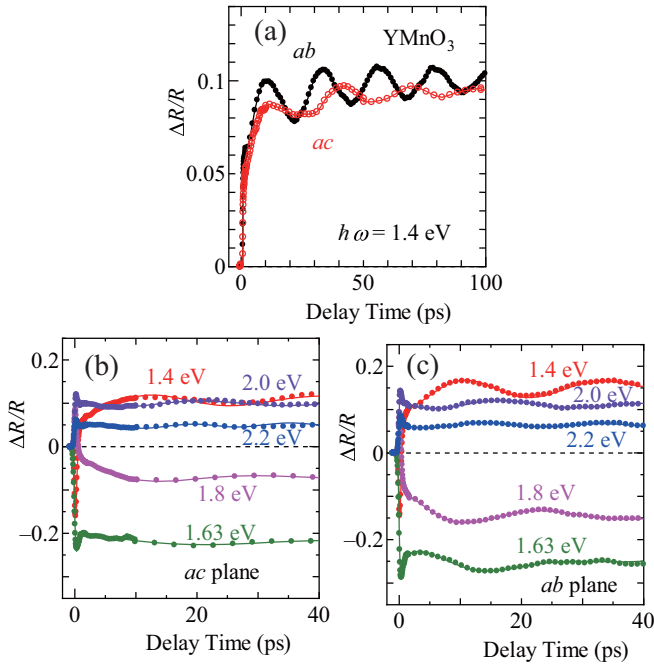


FIG. 8. (a) Photoinduced change in reflectivity $\Delta R/R$ as a function of the delay time t up to 100 ps measured on the ac (red) and ab (black) plane at $\hbar\omega = 1.4$ eV. (b),(c) Photoinduced change in the reflectivity $\Delta R/R$ as a function of the delay time t at various $\hbar\omega$ values of the probe pulse on the (b) ac and (c) ab planes up to 40 ps. Solid circles are the experimental results and solid lines are the results of the fitting using Eq. (5).

the difference in the oscillation period T in the t dependence of $\Delta R/R$.

The t dependence of $\Delta R/R$ up to 40 ps at various $\hbar\omega_{\text{probe}}$ values on the ab and ac planes is shown in Figs. 8(b) and 8(c). We fitted the t -dependent $\Delta R/R$ for $0 < t \leq 40$ ps using the following function:

$$\Delta R/R = C_0 + C_1 \exp\left(-\frac{t}{\tau_1}\right) + C_2 \exp\left(-\frac{t}{\tau_2}\right) \cos(At + \alpha). \quad (5)$$

Note that the oscillation period T is given by $2\pi/A$. We plot A obtained by the fitting as a function of $\hbar\omega_{\text{probe}}$ in Fig. 9(a). The dip of A as a function of $\hbar\omega_{\text{probe}}$ at ~ 1.8 eV seems to be correlated with a dip in the refractive index n as a function of $\hbar\omega_{\text{probe}}$ shown by a dashed line in the same graph, which was obtained by the Kramers-Kronig transformation of the reflectivity spectrum for the present YMnO_3 . Indeed, the sound velocity obtained by Eq. (4) using the experimentally obtained n [Fig. 9(b)] indicates that the values obtained by various $\hbar\omega_{\text{probe}}$ values are nearly the same, but there is a clear difference between the value along the a axis and that along the c axis. The sound velocity of YMnO_3 in the longitudinal mode along the a axis and that along the c axis were measured by a conventional technique to be 7.6×10^3 and 6.0×10^3 m/s² at 4 K, respectively [29]. The values obtained in the present experiment are consistent with these results.

Let us discuss $\Delta R/R$ up to several thousands of picoseconds (several nanoseconds). Figures 10(a)–10(c) show $\Delta R/R$

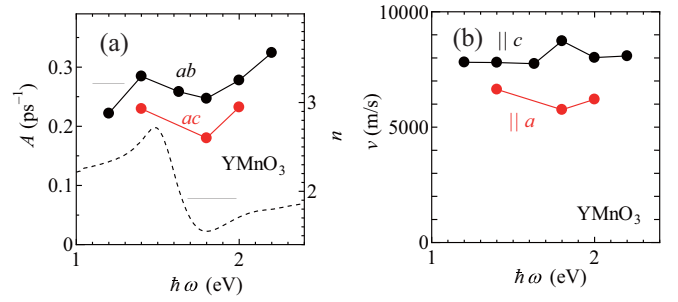


FIG. 9. (a) Frequency of oscillation in the t dependence of $\Delta R/R$, A , obtained by fitting using Eq. (5), as a function of $\hbar\omega$ of the probe pulse when the pulse is applied to the ac (red) and ab (black) planes for YMnO_3 . The dashed line corresponds to the refractive index n obtained by reflectivity measurement. (b) Sound velocities along the a (red) and c (black) axes for YMnO_3 obtained using Eq. (4).

as a function of t up to 5000 ps for $\hbar\omega_{\text{probe}} = 1.4, 1.63,$ and 2.0 eV. Here, $\Delta R/R$ at $t = 10$ ps is normalized to 1 or -1 for simplicity. As can be seen, $\Delta R/R$ gradually decreases with increasing t over thousands of picoseconds and the decrease is faster when the photoinduced $\Delta R/R$ is measured on the ab plane than on the ac plane.

The t dependence of $\Delta R/R$ in this range is likely dominated by thermal conduction. Namely, it is assumed that the complex dielectric constant ϵ of the sample changes

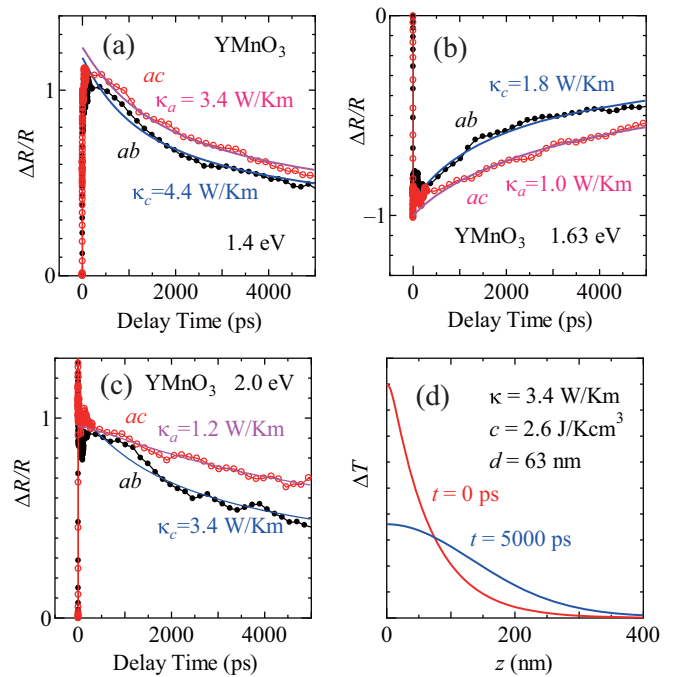


FIG. 10. (a)–(c) Photoinduced change in the reflectivity $\Delta R/R$ up to 5000 ps measured on the ac (red) and ab (black) planes at (a) 1.4, (b) 1.63, and (c) 2.0 eV of the probe pulse. The solid lines are the results of the fitting using Eqs. (6) and (7). (d) Temperature profile $T(z, t)$ with the parameters shown in the figure at $t = 0$ ps (red) and 5000 ps (blue), as an example.

proportionally to the change in its temperature:

$$\epsilon(T) = \epsilon(T_0) + \beta(T - T_0), \quad (6)$$

where T_0 is the base temperature. This assumption is justified by the linear dependence of $\Delta R/R$ on the intensity of the pump pulse, as described below. The temperature of the sample at time t and distance z from the sample surface [$T(z, t)$] is given by the thermal conduction equation

$$\kappa \frac{\partial^2 T(z, t)}{\partial z^2} = c \frac{\partial T(z, t)}{\partial t}, \quad (7)$$

where κ is the thermal conductivity and c is the specific heat of the sample. The initial $T(z, t)$ is determined by the heating caused by the pump pulse, which is given as

$$T(z, 0) = T_0 + a \exp\left(-\frac{z}{d}\right). \quad (8)$$

Here, d is the penetration depth of the pump pulse, which is determined by the extinction coefficient of the sample at the frequency of the pump pulse ($k = \text{Im}\sqrt{\epsilon}$) as $d = \lambda/4\pi k$, where λ is the wavelength of the pump pulse in vacuum (~ 795 nm). An example of $T(z, t)$ by the calculation is shown in Fig. 10(d).

Among various parameters, the ω -dependent complex dielectric constant ϵ can be obtained by the Kramers-Kronig transformation of the reflectivity spectrum. The complex number β in Eq. (6) was determined by measuring the reflectivity of YMnO₃ at a high temperature and obtaining the complex dielectric constant at that temperature by the Kramers-Kronig transformation. The specific heat c at room temperature for YMnO₃ is assumed as ~ 100 J/K mol = 2.6 J/K cm³ [31]. The constant a in Eq. (8) can be ignored if the concern is only the relative change in $\Delta R/R$ with t .

On the basis of these equations and parameters, $\epsilon(z, T) = \epsilon[T(z, t)]$ can be calculated. With this z -dependent complex dielectric constant, the reflectivity of the probe pulse at $\hbar\omega_{\text{probe}}$ can be calculated at each t . The thermal conductivity κ can be obtained by finding the value that can best reproduce the t dependence of $\Delta R/R$ up to 5000 ps. The results of the fitting are shown by dashed lines in Figs. 10(a)–10(c), together with the estimated κ values. As can be seen, at each $\hbar\omega_{\text{probe}}$, κ along the c axis (κ_c) is larger than that along the a axis (κ_a).

However, there are two problems with this result. First, the κ values obtained for different $\hbar\omega_{\text{probe}}$ values are quite different from each other. Second, the thermal conductivities at room temperature obtained by the conventional technique are ~ 8 W/K m along the c axis and ~ 5 W/K m along the a axis [30], which are clearly larger than those obtained by the pump-probe technique, although their anisotropy is correctly estimated.

For the latter problem, the effect of polishing can be a possible origin. Namely, since the thermal conductivity for a depth of only several hundreds of nanometers from the sample surface is measured in the present experiment, it can be affected by the polishing for the optical measurement, which can lead to the appearance of internal strains and defects, and the reduction in lattice thermal conductivity. For the former problem, we found that β in Eq. (6), particularly the ratio of the real to imaginary parts including its sign, strongly affects

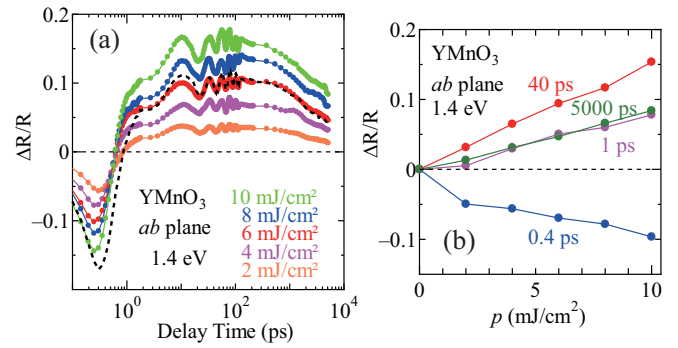


FIG. 11. (a) Photoinduced change in the reflectivity $\Delta R/R$ at $\hbar\omega = 1.4$ eV of the probe pulse on the ab plane as a function of the delay time t on a log scale at various values of the intensity of the pump pulse p . A dashed line is the data for $p = 2$ mJ/cm² multiplied by three. (b) $\Delta R/R$ at various values of t as a function of the intensity of the pump pulse p .

the thermal conductivity obtained by the fitting. We speculate that the fact that the thermal conductivity obtained by the measurement at $\hbar\omega_{\text{probe}} = 1.63$ eV is discernibly smaller than those obtained at other $\hbar\omega_{\text{probe}}$ values may be due to the error in estimating β at 1.63 eV, which is close to the peak in the optical conductivity.

Finally, let us see the dependence of $\Delta R/R$ on the intensity of the pump pulse. Figure 11(a) shows the photoinduced change in the reflectivity $\Delta R/R$ at $\hbar\omega = 1.4$ eV of the probe pulse as a function of the delay time t on a log scale at various values of the intensity of the pump pulse p . A dashed line is the data for $p = 2$ mJ/cm² multiplied by three. As can be seen, those data for $t > 1$ ps almost follow the data for $p = 6$ mJ/cm² but the data for $t < 1$ ps are substantially larger than those for $p = 6$ mJ/cm². Figure 11(b) shows $\Delta R/R$ at various values of t as a function of p . $\Delta R/R$ exhibits a saturation behavior with p for $t = 0.4$ ps but for other values of t , $\Delta R/R$ changes almost linearly with p . This means that the change in $\Delta R/R$ with an electronic origin exhibits a nonlinear behavior with respect to the intensity of the pump pulse, but once $\Delta R/R$ is dominated by the increase in lattice temperature, it becomes proportional to p , meaning that $\Delta R/R$ is proportional to the change in T .

IV. DISCUSSION

As described above, the change in reflectivity after the application of a pump pulse in hexagonal YMnO₃ from 0.1 to 5000 ps can be described by (1) the reconstruction of the electronic structure caused by the excitation of electrons by the pump pulse for $t < 1$ ps, (2) the increase in lattice temperature caused by the relaxation of the excited electrons to phonons for several picoseconds, (3) the propagation of the strain wave caused by the sudden increase in lattice temperature, resulting in the oscillation of reflectivity for several tens of picoseconds, and (4) the decrease in lattice temperature caused by the thermal conduction in the sample for several thousands of picoseconds. The above interpretations, particularly (3) and (4), have been further confirmed by the existence of the anisotropy with respect to the direction of the sample surface

on which the pump pulse is applied, which is consistent with the anisotropy measured by other techniques.

From the present experimental results, it was confirmed that even if the change in reflectivity is dominated by the electronic origin at the early stage of $t < 1$ ps, the energy in the electronic excitation is eventually transferred to phononic energy and, at the final stage, the change in reflectivity is dominated by the decrease in the temperature of the crystal through thermal conduction. Note that such a change in reflectivity associated with thermal conduction has been utilized to measure the thermal conductivity of thin films, called thermoreflectance [12–16]. Thus far, however, it has not been clarified how such a phenomenon occurring on the time scale of longer than nanoseconds is related to the photoinduced process occurring on the time scale of picoseconds or shorter. The present experiments clearly demonstrate a coherent transition from the change with an electronic origin to a change caused by thermal process in YMnO_3 .

Note that the present compound does not exhibit a photoinduced phase transition. If it does, the dynamics of the domain walls between the two competing phases will contribute to the time dependence of reflectivity and this may cause a longer time dependence. Indeed, for perovskite manganites near the ferromagnetic transition temperature, where a ferromagnetic state and a paramagnetic state with short-range charge/orbital ordering are competing, the time dependence of reflectivity from microseconds to milliseconds was detected by an optical technique [32]. The relationship between the photoinduced phase transition and such dynamics of the domain walls should be clarified in the future.

It should also be emphasized that the present experimental technique is useful for easily obtaining the sound velocity and thermal conductivity of materials including their anisotropy. In particular, the discrepancy between the absolute values of the sound velocity obtained by the present technique and that by the conventional technique is within 20%, indicating that it can be used as an easy way to quantitatively measure the sound velocity of materials, whose size may be too small to measure it by a conventional technique. It should also be pointed out that such a technique, which is related to the processes (3) and (4) above, can be commonly used for any kinds of materials, from metals to insulators. On the other hand, the processes (1) and (2) strongly depend on the characteristics of the materials; the process (1) in YMnO_3 is dominated by the fact that the peak arises from the $d-d$ excitation of the Mn ions, which is coupled with the charge-transfer excitation. The process (2) is related to the fact that the excitation energy of

the $d-d$ excitation shifts to the lower energy with increasing T . In other words, processes (1) and (2) can be used to clarify the characteristics of the electronic structure for specific materials.

V. SUMMARY

Pump-probe optical spectroscopy over a wide time scale range from 0.1 to 5000 ps and over a wide $\hbar\omega$ range from 1 to 3 eV was conducted on hexagonal YMnO_3 , where a sharp peak at 1.6 eV arising from a $d-d$ excitation of Mn^{3+} ions dominates the optical spectrum. It was found that the change in reflectivity is such that (1) the broadening of the peak for the $d-d$ excitation in less than 1 ps, (2) the recovery of the width and the shift of the peak to lower frequencies for several ps, (3) an oscillation in reflectivity with a period of several tens of picoseconds, and (4) a decrease in the absolute value of the reflectivity change over several thousands of picoseconds. The broadening of the $d-d$ excitation peak can be explained by the coupling of the excitation with the charge-transfer excitation between the oxygen $2p$ state and the Mn $3d$ state. The peak shift can be explained by the increase in lattice temperature caused by the relaxation of energy from the excitation of electrons to that of phonons, i.e., Joule heating. The oscillation of reflectivity can be explained by the interference of the light reflected at the surface and the wave front of the strain wave that appears near the sample surface and propagates through sound velocity. The decrease in the absolute value of the reflectivity change occurs because the sample approaches a thermally equilibrium state owing to the thermal conduction inside the sample. For the processes dominated by sound velocity and thermal conductivity, the anisotropy with respect to the direction of the sample surface is experimentally observed. The present experimental results indicate that in pump-probe spectroscopy, even if a process occurring faster than 1 ps has an electronic origin, a slower process is dominated by the increase in lattice temperature due to the Joule heating of the sample and the decrease in lattice temperature caused by thermal conduction. The present experiments also demonstrate that pump-probe spectroscopy is a useful technique for simultaneously obtaining sound velocity and thermal conductivity.

ACKNOWLEDGMENT

This work was supported by JSPS KAKENHI Grants No. 22H01172 and No. 22H04484.

-
- [1] M. F. Becker, A. B. Buckman, R. M. Walser, T. Lépine, P. Georges, and A. Brun, Femtosecond laser excitation of the semiconductor-metal phase transition in VO_2 , *Appl. Phys. Lett.* **65**, 1507 (1994).
 [2] A. Cavalleri, C. Tóth, C. W. Siders, J. A. Squier, F. Ráksi, P. Forget, and J. C. Kieffer, Femtosecond Structural Dynamics in VO_2 during an Ultrafast Solid-Solid Phase Transition, *Phys. Rev. Lett.* **87**, 237401 (2001).
 [3] M. Chollet, L. Guerin, N. Uchida, S. Fukaya, H. Shimoda, T. Ishikawa, K. Matsuda, T. Hasegawa, A. Ota, H. Yamochi,

G. Saito, R. Tazaki, S. Adachi, and S. Koshihara, Gigantic photoresponse in 1/4-filled-band organic salt $(\text{EDO-TTF})_2\text{PF}_6$, *Science* **307**, 86 (2005).

- [4] S. Iwai and H. Okamoto, Ultrafast phase control in one-dimensional correlated electron systems, *J. Phys. Soc. Jpn.* **75**, 011007 (2006).
 [5] M. Rini, R. Tobey, N. Dean, J. Itatani, Y. Tomioka, Y. Tokura, R. W. Schoenlein, and A. Cavalleri, Control of the electronic phase of a manganite by mode-selective vibrational excitation, *Nature (London)* **449**, 72 (2007).

- [6] H. Yamakawa, T. Miyamoto, T. Morimoto, T. Terashige, H. Yada, N. Kida, M. Suda, H. M. Yamamoto, R. Kato, K. Miyagawa, K. Kanoda, and H. Okamoto, Mott transition by an impulsive dielectric breakdown, *Nat. Mater.* **16**, 1100 (2017).
- [7] T. Saiki, N. Yamaguchi, Y. Obata, Y. Kakesu, T. Kajita, and T. Katsufuji, Photoinduced phase transitions over three phases in $\text{Ba}_{0.9}\text{Sr}_{0.1}\text{V}_{13}\text{O}_{18}$, *Phys. Rev. B* **96**, 035133 (2017).
- [8] T. Saiki, T. Yoshida, K. Akimoto, D. Indo, M. Arizono, T. Okuda, and T. Katsufuji, Selection rule for the photoinduced phase transition dominated by anisotropy of strain in Ti_3O_5 , *Phys. Rev. B* **105**, 075134 (2022).
- [9] C. Thomsen, H. T. Grahn, H. J. Maris, and J. Tauc, Surface generation and detection of phonons by picosecond light pulses, *Phys. Rev. B* **34**, 4129 (1986).
- [10] Y. Okimoto, X. Peng, M. Tamura, T. Morita, K. Onda, T. Ishikawa, S. Koshihara, N. Todoroki, T. Kyomen, and M. Itoh, Ultrasonic Propagation of a Metallic Domain in $\text{Pr}_{0.5}\text{Ca}_{0.5}\text{CoO}_3$ Undergoing a Photoinduced Insulator-Metal Transition, *Phys. Rev. Lett.* **103**, 027402 (2009).
- [11] K. Takubo, Y. Onishi, A. Furuhashi, A. Nogami, and T. Katsufuji, Photoinduced dynamics of spinel MnV_2O_4 , *Phys. Rev. B* **88**, 214416 (2013).
- [12] D. G. Cahill, W. K. Ford, K. E. Goodson, G. D. Mahan, A. Majumdar, H. J. Maris, R. Merlin, and A. R. Phillpot, Nanoscale thermal transport, *J. Appl. Phys.* **93**, 793 (2003).
- [13] P. M. Norris, A. P. Caffrey, R. J. Stevens, J. M. Klopff, and J. T. M. J. A. Smith, Femtosecond pump-probe nondestructive examination of materials, *Rev. Sci. Instrum.* **74**, 400 (2003).
- [14] D. G. Cahill, Analysis of heat flow in layered structures for time-domain thermoreflectance, *Rev. Sci. Instrum.* **75**, 5119 (2004).
- [15] C. Chiritescu, D. G. C. N. Nguyen, D. Johnson, A. Bodapati, P. Keblinski, and P. Zschack, Ultralow thermal conductivity in disordered, layered WSe_2 crystals, *Science* **315**, 351 (2007).
- [16] T. Katsufuji, T. Saiki, S. Okubo, Y. Katayama, and K. Ueno, Thermal conductivity of SrVO_3 - SrTiO_3 thin films: Evidence of intrinsic thermal resistance at the interface between oxide layers, *Phys. Rev. Mater.* **2**, 051002(R) (2018).
- [17] D. Fröhlich, S. Leute, V. V. Pavlov, and R. V. Pisarev, Nonlinear Optical Spectroscopy of the Two-Order-Parameter Compound YMnO_3 , *Phys. Rev. Lett.* **81**, 3239 (1998).
- [18] T. Katsufuji, S. Mori, M. Masaki, Y. Moritomo, N. Yamamoto, and H. Takagi, Dielectric and magnetic anomalies and spin frustration in hexagonal RMnO_3 ($\text{R}=\text{Y}$, Yb , and Lu), *Phys. Rev. B* **64**, 104419 (2001).
- [19] T. Katsufuji, M. Masaki, A. Machida, M. Moritomo, K. Kato, E. Nishibori, M. Takata, M. Sakata, K. Ohoyama, K. Kitazawa, and H. Takagi, Crystal structure and magnetic properties of hexagonal RMnO_3 ($\text{R}=\text{Y}$, Lu , and Sc) and the effect of doping, *Phys. Rev. B* **66**, 134434 (2002).
- [20] A. B. Souchkov, J. R. Simpson, M. Quijada, H. Ishibashi, N. Hur, J. S. Ahn, S. W. Cheong, A. J. Millis, and H. D. Drew, Exchange Interaction Effects on the Optical Properties of LuMnO_3 , *Phys. Rev. Lett.* **91**, 027203 (2003).
- [21] S.-T. Lou, F. M. Zimmermann, R. A. Bartynski, N. Hur, and S.-W. Cheong, Femtosecond laser excitation of coherent optical phonons in ferroelectric LuMnO_3 , *Phys. Rev. B* **79**, 214301 (2009).
- [22] K.-J. Jang, J. Lim, J. Ahn, J.-H. Kim, K.-J. Yee, J. S. Ahn, and S.-W. Cheong, Ultrafast ir spectroscopic study of coherent phonons and dynamic spin-lattice coupling in multiferroic LuMnO_3 , *New J. Phys.* **12**, 023017 (2010).
- [23] K.-J. Jang, H.-G. Lee, S. Lee, J. Ahn, J. S. Ahn, N. Hur, and S.-W. Cheong, Strong spin-lattice coupling in multiferroic hexagonal manganite YMnO_3 probed by ultrafast optical spectroscopy, *Appl. Phys. Lett.* **97**, 031914 (2010).
- [24] K. H. Wu, H.-J. Chen, Y. T. Chen, C. C. Hsieh, C. W. Luo, T. M. Uen, J. Y. Juang, J.-Y. Lin, T. Kobayashi, and M. Gospodinov, Marked enhancement of Néel temperature in strained YMnO_3 thin films probed by femtosecond spectroscopy, *Europhys. Lett.* **94**, 27006 (2011).
- [25] Z. Jin, H. Ma, G. Li, Y. Xu, G. Ma, and Z. Cheng, Ultrafast dynamics of the Mn^{3+} d-d transition and spin-lattice interaction in YMnO_3 film, *Appl. Phys. Lett.* **100**, 021106 (2012).
- [26] Y. T. Wang, C. W. Luo, and T. Kobayashi, Understanding multiferroic hexagonal manganites by static and ultrafast optical spectroscopy, *Adv. Condens. Matter Phys.* **2013**, 104806 (2013).
- [27] T. Hasegawa, N. Fujimura, and M. Nakayama, Ultrafast dynamics of coherent optical phonon correlated with the anti-ferromagnetic transition in a hexagonal YMnO_3 epitaxial film, *Appl. Phys. Lett.* **111**, 192901 (2017).
- [28] W.-H. Huang, H.-K. Wei, N. N. Quyen, P.-T. Yang, Y.-C. Cheng, Y.-T. Wang, Y.-K. Ko, C.-M. Tu, A. Yabushita, and C.-W. Luo, Energy-resolved ultrafast spectroscopic investigation on the spin-coupled electronic states in multiferroic hexagonal HoMnO_3 , *Materials* **15**, 5188 (2022).
- [29] M. Poirier, F. Laliberté, L. Pinsard, and A. Revcolevschi, Magnetoelastic coupling in hexagonal multiferroic YMnO_3 using ultrasound measurements, *Phys. Rev. B* **76**, 174426 (2007).
- [30] P. A. Sharma, J. S. Ahn, N. Hur, S. Park, S. B. Kim, S. Lee, J.-G. Park, S. Guha, and S.-W. Cheong, Thermal Conductivity of Geometrically Frustrated, Ferroelectric YMnO_3 Extraordinary Spin-Phonon Interactions, *Phys. Rev. Lett.* **93**, 177202 (2004).
- [31] M. Tachibana, J. Yamazaki, H. Kawaji, and T. Atake, Heat capacity and critical behavior of hexagonal YMnO_3 , *Phys. Rev. B* **72**, 064434 (2005).
- [32] J. Masuzawa, Y. Saiki, T. Suzuki, and T. Katsufuji, Study of dynamics in inhomogeneous states by temperature-modulated optical reflectivity measurement: Application to perovskite manganites, *J. Phys. Soc. Jpn.* **79**, 014704 (2010).